

# Influence of the dispersive properties of metals on the transmission characteristics of left-handed materials

N.-C. Panoiu<sup>1,\*</sup> and R. M. Osgood, Jr.<sup>2</sup>

<sup>1</sup>*Department of Applied Physics and Applied Mathematics, Columbia University, New York, New York 10027, USA*

<sup>2</sup>*Brookhaven National Laboratories, Upton, New York 11973, USA*

*and Department of Applied Physics and Applied Mathematics, Columbia University, New York, New York 10027, USA*

(Received 16 January 2003; revised manuscript received 24 March 2003; published 21 July 2003)

We study numerically the influence of the frequency dispersion of the dielectric function of metals on the physical properties of negative-refractive-index metamaterials. A numerical analysis is performed using the transfer matrix formalism in conjunction with the finite-difference time-domain method. We analyze the dependence of the transmission and absorption properties of a slab of split-ring-type resonators on the parameters characterizing the frequency dispersion of the metallic dielectric function: plasma frequency and damping frequency. Then, using these transmission and reflection coefficients, we show that the refractive index remains negative near the resonant frequency of the rings, despite the presence of frequency dispersion. We also determine the dependence of the position and width of the band gaps of a slab of such a metamaterial on the material dispersion. Finally, we also discuss the influence of the shape of the split-ring resonators on the transmission and reflection coefficients. The calculations are performed for both two- and three-dimensional structures.

DOI: 10.1103/PhysRevE.68.016611

PACS number(s): 42.25.Bs, 42.70.Qs, 41.20.Jb

## I. INTRODUCTION

More than three decades ago, Veselago described theoretically the electromagnetic properties of a medium, for which both the electric permittivity  $\epsilon$  and the magnetic permeability  $\mu$  are negative [1]. Thus, he predicted that this property would lead to very unusual characteristics of the propagation of electromagnetic waves in such a medium: reverse of Snell's law (that is, such media behave as if they had a negative refractive index), reversed Doppler shift, backward emission of Cherenkov radiation, negative radiation pressure, etc. However, since for ordinary materials  $\epsilon$  and  $\mu$  are not simultaneously negative, these theoretical predictions could not be verified experimentally until recently. Since in these media the electric field, magnetic field, and the propagation wave vector of an electromagnetic plane wave form a left-handed system of vectors, such media have been named left-handed materials (LHM).

Very recently, the fabrication of materials, which exhibit the properties of a LHM at frequencies in the microwave region, has been reported [2–5]. The central ideas that led to the choice of the structure of the metamaterials introduced in Ref. [2] can be traced to the work of Pendry *et al.* [6–8]. Thus, in Ref. [6] it has been suggested that, in the microwave region, a lattice of metallic split-ring resonators (SRR) with characteristic features in the millimeter range behaves as an effective medium which has a negative magnetic permeability  $\mu_{\text{eff}}$ . The main factor which determines this behavior is that the resonant frequency of these specially designed SRR corresponds to a wavelength that is several times larger than the lattice constant. Thus, the effective medium approximation is valid and theoretical calculations have shown that the

corresponding  $\mu_{\text{eff}}$  is negative. Furthermore, in Refs. [7–9] it was also demonstrated that a network of thin metallic wires behaves as a quasimetal with a highly reduced plasma frequency. A consequence of this phenomenon is that the penetration depth of electromagnetic waves in such a quasimedium is increased considerably. By combining these two structures, Smith *et al.* [2] have demonstrated that one can fabricate a metamaterial which, within a certain frequency range, has both  $\epsilon$  and  $\mu$  negative, that is, a LHM.

Although some of the properties of LHM are still not fully understood [10–14], they offer a rich ground for both theoretical and, recently, experimental researches. Thus, surface polaritons of a LHM [15], scattering properties of LHM spheres [16] or cylinders [17], or the properties of electromagnetic wave propagation in LHM [18] have been studied theoretically, whereas their transmission properties have been investigated experimentally [2,19].

Despite the fact that LHM could have important technological applications in the microwave regime (antenna, selective reflective surfaces), it would also be important if one could fabricate LHM at infrared or optical frequencies. Although several candidates for LHM at optical frequencies have been proposed [20–22], to the best of our knowledge, this paper is the first attempt to extend the analysis of the properties of LHM proposed by Smith *et al.* at infrared and optical frequencies. There are several reasons why this extension cannot be made simply by scaling down the characteristic dimensions of the building blocks of the LHM. First, as the frequency approaches the optical spectrum, the frequency dispersion of the dielectric function of the metal becomes important and cannot be neglected. Second, it is well known that as the frequency becomes comparable to the plasma frequency, surface plasmons are excited, leading to significant changes of the electromagnetic properties of the metallic structures [23,24].

---

\*Electronic address: panoiu@cumsl.msl.columbia.edu

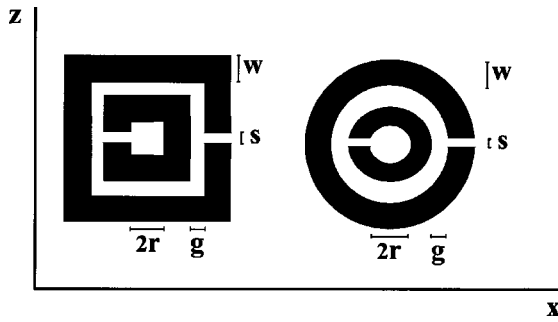


FIG. 1. The structure of a hollow square (left) and circular (right) split-ring resonator with an inner (core) radius  $r=1 \mu\text{m}$ , gap  $g=0.33 \mu\text{m}$ , split  $s=0.4 \mu\text{m}$ , and width  $w=0.33 \mu\text{m}$ .

The importance of this work is twofold. First, as just mentioned, it extends the analysis of the LHM to the infrared and optical frequencies, a region that could offer important technological applications. Second, since the periodic distribution of SRR and thin metallic wires can be viewed as a photonic crystal, this work is of interest for the understanding of the physical properties of the metallic photonic band gap (PBG) materials at optical frequencies. Thus, until recently, most of the research work on the PBG materials focused on photonic crystals consisting of dielectrics. However, recent research studies have shown that it is possible to design metallic photonic crystals with new features: large relative gap width [25,26], unusual transmission properties [27,28], or high surface impedance [29].

The paper is organized as follows. In Sec. II, we briefly describe the structure of the unit cell of the LHM. Then, in Sec. III, we introduce two numerical methods, used here: the transfer matrix method (TMM) and the finite-difference time-domain (FDTD) method. Furthermore, in Sec. IV we present our results obtained by analyzing the transmission and reflection coefficients of a slab of material can be used to determine its effective permittivity, effective permeability, and refractive index and apply this method to the LHM. Finally, in Sec. V our results are summarized and discussed.

## II. DESCRIPTION OF THE UNIT CELL OF THE LHM

The LHM introduced in Ref. [2] consists of two interspersed periodic metallic structures. The first one is a periodic lattice of metallic SRR with either a circular or a rectangular shape. The geometrical features of such a structure are presented in Fig. 1. Note that throughout this paper, the characteristic dimensions of our structures were chosen to be near the fabrication limit of current industry patterning technology, that is, a few hundred nanometers.

Although not unique, the geometry in Fig. 1 has several features that make it an ideal candidate for the building block of a LHM. Thus, the small gap between the two rings creates a large capacitance which, combined with the inductance of the rings, lowers considerably their combined resonant frequency. Furthermore, the split of the rings ensures that the resonant frequency corresponds to a wavelength several times larger than the diameter of the rings. Had the rings

been continuous, the resonant wavelength would have been equal to their diameter. Thus, one can treat the periodic lattice within the effective medium approximation. Moreover, since the rings are magnetically active, resonant behavior can be induced only by  $s$ -polarized electromagnetic waves, that is, waves with the magnetic field along the ring's axis.

Theoretical calculations using a nondispersive metal have shown that a periodic lattice made from SRR is characterized by an effective magnetic permeability given by the following analytic expression [6]:

$$\mu_{\text{eff}} = 1 - \frac{F\omega^2}{\omega^2 - \omega_0^2 + i\Gamma\omega}, \quad (1)$$

where  $F = \pi r^2/a^2$  is the fill factor,

$$\omega_0^2 = \frac{3lc^2}{\pi r^3 \ln \frac{2w}{g}} \quad (2)$$

is the resonant frequency, and

$$\Gamma = \frac{2\rho l}{\mu_0 r} \quad (3)$$

is the resonance width. In Eqs. (2) and (3),  $a$  is the lattice constant,  $r$  is the inner radius of the ring,  $w$  is the width of the rings,  $l$  is the distance between adjacent planes of SRR, and  $\rho$  is the resistance per unit length of the rings measured along the circumference.

The second component of the LHM introduced in Ref. [2] consists of a network of thin metallic wires which acts as a high-pass filter: only the frequencies above a cutoff threshold (the plasma frequency of the quasimetal-type medium) can propagate in the material. Since the cutoff frequency corresponds to a wavelength several times larger than the period of the structure, again the effective medium approximation holds. The effective dielectric function of this quasimedium can be written as [7,8]

$$\epsilon_{\text{eff}} = 1 - \frac{\tilde{\omega}_p^2}{\omega(\omega + i\tilde{\gamma})}, \quad (4)$$

where  $\tilde{\omega}_p$  is the associated plasma frequency of the longitudinal modes and  $\tilde{\gamma}$  plays the role of absorption.

## III. NUMERICAL METHODS

In analyzing the transmission properties of a slab of LHM, we used two numerical methods: TMM and FDTD. The first method is extremely useful in determining the scattering properties of periodic structures, whereas the latter can offer valuable insights into the time evolution of the solutions of Maxwell's equations in a finite spatial domain. In this section, we will briefly describe both these methods.

### A. Transfer matrix method

The TMM, which was introduced by Pendry and co-workers [30,31], is a powerful tool for calculating the band structure of periodic dielectric materials. This method has been used for investigating periodic metallic structures both at microwave [32,33] and optical [34] frequencies. It consists of discretizing Maxwell's equations on a lattice containing the unit cell of the periodic structure and then constructing the transfer matrix that relates the electromagnetic fields at the input and output facets of the unit cell. Thus, if one considers that the output field  $\mathcal{F}_{\text{out}}$  is related to the input field  $\mathcal{F}_{\text{in}}$  through the relation

$$\mathcal{F}_{\text{out}} = \mathbf{T}\mathcal{F}_{\text{in}}, \quad (5)$$

where  $\mathbf{T}$  is the transfer matrix of the unit cell, one can easily prove that the matrix  $\mathbf{T}$  can be written as [30,31]

$$\mathbf{T} = \begin{pmatrix} t_{++} - t_{+-}(t_{--})^{-1}t_{-+} & t_{+-}(t_{--})^{-1} \\ -(t_{--})^{-1}t_{-+} & (t_{--})^{-1} \end{pmatrix}. \quad (6)$$

The parameter  $t_{++}$  ( $t_{--}$ ) represents the transmission coefficient of a wave incoming from the left (right) and transmitted to the right (left),  $t_{-+}$  ( $t_{+-}$ ) represents the reflection coefficient of a wave incoming from the left (right) and reflected to the left (right), and  $t_{++}$ ,  $t_{--}$ ,  $t_{-+}$ , and  $t_{+-}$  being the elements of the scattering matrix  $\mathbf{S}$  that relates the incoming and outgoing waves:

$$\mathbf{S} = \begin{pmatrix} t_{++} & t_{+-} \\ t_{-+} & t_{--} \end{pmatrix}. \quad (7)$$

One of the advantages of using the TMM formalism is that it allows one to decompose large structures, for which the transfer matrix could be difficult to calculate, into smaller ones which can be calculated easily. Then, from these matrices, one calculates the transfer matrix for the entire structure. The reason why this approach works is that the transfer matrix obeys the following composition rule:

$$\mathbf{T}_{12} = \mathbf{T}_2\mathbf{T}_1, \quad (8)$$

where  $\mathbf{T}_1$  and  $\mathbf{T}_2$  are the transfer matrices of two adjacent layers and  $\mathbf{T}_{12}$  is the transfer matrix of the combined layer.

However, repeated use of the Eq. (8) can soon lead to numerical instabilities. As we add new layers, the numerical instabilities in the transfer matrix accumulate, leading to massive computational problems. To overcome this problem, instead of using Eq. (8) to account for the combined effect of two layers of the material, we used a similar expression, except that we construct the *scattering* matrix of an ensemble of two layers from the *scattering* matrices of each layer. The advantage of this approach is that the elements of the scattering matrix are of the order of unity; consequently, when applied to scattering matrices, this recursive process is numerically stable (for details, see Ref. [31]). The drawback is that computing the scattering matrix of two layers by using the scattering matrix of each layer is computationally an expensive operation. Therefore, in practice one calculates first

the transfer matrices for subsystems that are as large as possible; then one determines the scattering matrices for these subsystems; and finally, from these scattering matrices, one calculates the scattering matrix for the entire system.

One final modification of the previous algorithm is needed when dealing with periodic structures with large absolute values of the dielectric constants (as it is the case with metallic structures). In this case, to avoid numerical instabilities, it is necessary to subpartition even the unit cell and to calculate first the transfer matrix for each subpartition.

Another advantage of the TMM is that it allows one to describe periodic structures made from materials characterized by frequency-dependent parameters, i.e., dispersion. This feature is especially useful when investigating metallic structures at optical frequencies. The reason for this is that TMM, unlike other widely used methods, e.g., plane wave expansion method, operates at fixed frequencies. Therefore, even if one deals with dispersive materials, the transmission and reflection coefficients or the band structure of periodic structures can still be computed by means of TMM.

### B. Finite-difference time-domain method

FDTD is the second method used here. It was introduced in Ref. [35] and involves solving Maxwell's equations on a spatial grid that contains the structure of interest. Since the FDTD method is well known and widely used in many areas of computational electromagnetic modeling, we present here only those features concerning its application to structures containing frequency-dependent materials. For a detailed presentation of the FDTD, see Ref. [36].

In order to model the frequency-dependent response of the real material, i.e., the metal in the wires or rings, we assume that its dielectric function  $\epsilon(\omega)$  can be described by a single Lorentzian,

$$\epsilon = 1 - \frac{(\epsilon_s - 1)\omega_0^2}{\omega^2 - \omega_0^2 + 2i\delta\omega}, \quad (9)$$

where  $\epsilon_s$  is the static value of the dielectric constant,  $\omega_0$  is the resonant frequency, and  $\delta$  is the damping frequency. Once the frequency-domain representation of the dielectric constant is set by the Eq. (9), one can easily obtain, by the Fourier transformation, the time dependence of the susceptibility  $\chi(t)$  and, consequently, the functional relationship between the electric flux density  $\mathbf{D}(t)$  and the electric field  $\mathbf{E}(t)$ . Since the medium is dispersive, this relationship is nonlocal in time. The Yee algorithm must then be modified to take into account this nonlocal relationship between  $\mathbf{D}(t)$  and  $\mathbf{E}(t)$  [36].

However, the physical parameter that is generally used to describe the optical properties of a metal and is directly measured experimentally is the refractive index  $n$ . Thus, we took it as the basic input parameter for the FDTD based computations. The parameters  $\epsilon_s$  and  $\delta$  are then determined from the Eq. (9) by fixing the refractive index

$$n(\omega) \equiv n_r(\omega) + i \frac{\alpha(\omega)}{2} \equiv \sqrt{\epsilon(\omega)} \quad (10)$$

at some reference frequency  $\omega_{\text{ref}}$ . Here,  $n_r$  and  $\alpha$  represent the real part of the refractive index and absorption, respectively. Finally, the resonant frequency  $\omega_0$  is chosen to be a certain fraction of the reference frequency  $\omega_{\text{ref}}$  and its specific value does not affect the results of the computations as long as it is chosen far enough from the reference frequency  $\omega_{\text{ref}}$  [37].

In all the FDTD based numerical computations we used FULLWAVE, a commercially available software [38].

#### IV. TRANSMISSION THROUGH A SLAB OF LHM

In this section we present the main results regarding the transmission and absorption properties of a slab of LHM at infrared and optical frequencies. We start by discussing the results obtained by the TMM and conclude by presenting both the transmission properties of a full three-dimensional (3D) slab of LHM as well as the corresponding structures of the electromagnetic field. The latter are obtained by the FDTD method.

##### A. TMM based computations

As has been pointed out in earlier studies of the LHM based on interspersed SRR and thin wires, the main factor that determines the properties of the material (e.g., the frequency at which it exhibits a negative refractive index, the value of the index, etc.) is the geometry of the SRR. Therefore, we will analyze in detail the relationship between the characteristics of the SRR and the properties of the LHM.

Due to the fact that full 3D numerical simulations using the TMM are extremely time consuming, we used this method to investigate only the 2D case. Thus, the SRR are replaced by a periodic distribution of infinite split cylinders. The advantage offered by this choice is that we could use a much finer computational grid, increasing thus the accuracy of the results. Furthermore, as has been proven in Ref. [6], such geometry leads to a similar resonant behavior as in the case of SRR and the effective permeability is given by a formula similar to Eq. (1). In fact, Eq. (1) has been derived under the assumption that the magnetic field in a lattice of SRR is identical to the one in a periodic distribution of split cylinders [6]. When the SRRs are replaced by infinite cylinders, the parameters  $\omega_0$  and  $\Gamma$  in Eqs. (2) and (3) change to  $\omega_0^2 = 3\omega c^2 / \pi^2 r^3$  and  $\Gamma = 2\rho' / \mu_0 r$ , where  $\rho'$  is the resistance per unit area [6].

In order to calculate the transmission properties through a slab of such split cylinders, we proceeded as follows. First, we chose the unit cell as the domain containing one split cylinder and covered it with a mesh of  $N \times N$  points. Then, the unit cell was further divided into  $K$  subdomains (in most of the calculations, we chose  $K=5$ ) and for each subdomain, we computed the scattering matrix. From these matrices, by using the procedure discussed in Sec. III, we subsequently calculated the scattering matrix for the entire unit cell. The value of the number of discretization points,  $N$ , was increased until the transmission coefficient would no longer change. Generally,  $N=30$  was enough. Finally, layers con-

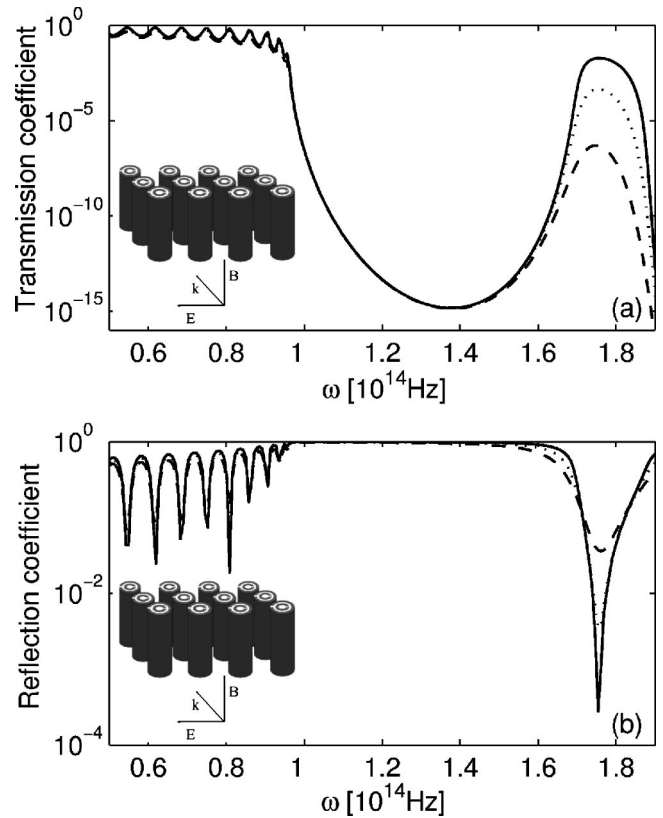


FIG. 2. The transmission coefficient (a) and reflection coefficient (b) for a slab of  $M=16$  layers of split cylinders. The plasma frequency is  $\omega_p = 7.5 \times 10^{15}$  Hz, the damping frequency  $\gamma = 10^{13}$  Hz (continuous line),  $\gamma = 2 \times 10^{13}$  Hz (dotted line), and  $\gamma = 4 \times 10^{13}$  Hz (dashed line). The parameters of the split cylinders are the same as those in Fig. 1 and the lattice constant is  $a = 5 \mu\text{m}$ .

taining one unit cell were stacked together to form slabs of the desired thickness.

As shown in the sketch in Fig. 2, the incident wave was taken to be perpendicular on the axis of the cylinders. Along the transverse direction, with respect to the incident wave, the slab is infinite since along this direction we imposed periodic boundary conditions. In this geometry, two polarizations of the incident wave are of interest:  $s$  polarization when the *magnetic* field is along the cylinder axis and  $p$  polarization when the *electric* field is along the cylinder axis. It has been pointed out in previous studies [2,32,33] that only in the first case does the material exhibit a negative refractive index. We determined the transmission properties of the slab for both polarizations.

Since we deal with metallic structures and the frequency is in the infrared to optical region, the metal must be considered to be dispersive, that is, the dielectric constant of the metal structures is frequency dependent. More exactly, we assumed that the real metal can be described by a Drude-like model,

$$\epsilon_m = 1 - \frac{\omega_p^2}{\omega(\omega + i\gamma)}, \quad (11)$$

where  $\omega_p$  is the plasma frequency and  $\gamma$  is the damping

frequency related to optical absorption in the metal. The Drude expression is a good approximation for most common metals [39] and, thus, using Eq. (11) allows us to incorporate realistic dispersive effects in our calculations. Notice the difference between Eqs. (4) and (11): while in Eq. (4)  $\epsilon_{\text{eff}}$  represents the effective dielectric function of the network of metallic wires, calculated within the effective medium approximation, Eq. (11) gives the intrinsic dielectric function of the actual metal.

We used this expression for the dielectric function of the metal and calculated the transmission and reflection coefficients through a slab of  $M = 16$  layers of SRR (see sketch in Fig. 2). The results for the  $s$  polarization of the incident wave are presented in Fig. 2. Our numerical simulations revealed several phenomena. First, there are multiple gaps in the transmission coefficient, the first, shown in Fig. 2, being at about  $1.2 \times 10^{14}$  Hz. The corresponding wavelength is about  $\lambda \approx 15 \mu\text{m}$ , that is, about three times the lattice constant  $a$ . Therefore, one expects that for frequencies within this range the effective medium approximation holds, such that it is meaningful to introduce an effective permeability. Moreover, for the frequency range shown in Fig. 2, there exists only one nonzero wave vector, that is, there exists only one mode, evanescent or propagating. All the other band gaps (not shown here) correspond to wavelengths that are *comparable or smaller* than the lattice constant or even the diameter of the cylinders, so that for these wavelengths the effective medium approximation is not valid. Therefore, we will focus on the properties of the first band gap. Moreover, the very small values of the calculated transmission coefficients near the center of the band gaps, which are only computationally meaningful for an idealized geometry, are just a manifestation of how the TMM builds the transmission-reflection coefficients of a thin layer of material into the transmission-reflection coefficients of a larger slab of material.

One important characteristic of this band gap is that it has a rather large relative gap width  $g_w$ , defined as the ratio between the gap width and its midgap frequency. For the case presented in Fig. 2,  $g_w \approx 55\%$ . The transmission and reflection coefficients presented in Fig. 2 are calculated for several values of the damping frequency  $\gamma$ . We observed that, as  $\gamma$  increases, i.e., the metal is more lossy, the depth in the transmission gaps decreases; however, the general structure and the position of these gaps remain unchanged. Also, notice the Fabry-Perot resonances at frequencies less than those corresponding to the first gap: these arise from the interference between the forward and backward propagating waves into the slab.

Finally, we point out that for  $p$  polarization no frequency gaps have been observed within this frequency range and that, within machine precision, for this polarization the transmission coefficient was equal to zero. This proves that the gaps are magnetically induced.

We also determined the absorption properties of a slab of split cylinders, and the results are illustrated in Fig. 3. Here we show a larger domain of frequencies, such that more gaps are seen in this figure. As this figure shows, as the damping frequency  $\gamma$  increases the absorption of the slab increases; this absorption is larger at frequencies that correspond to

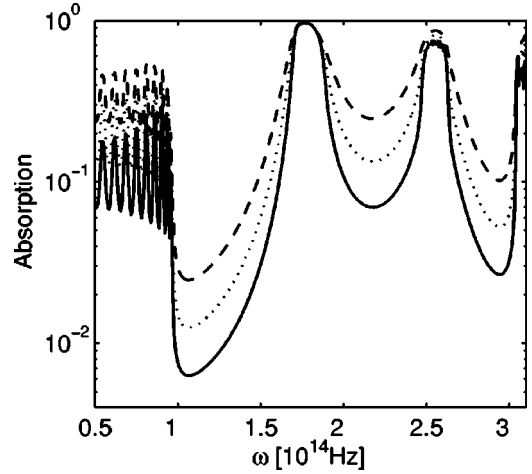


FIG. 3. The absorption coefficient for a slab of  $M = 16$  layers of split cylinders. The plasma frequency is  $\omega_p = 7.5 \times 10^{15}$  Hz, the damping frequency  $\gamma = 10^{13}$  Hz (continuous line),  $\gamma = 2 \times 10^{13}$  Hz (dotted line), and  $\gamma = 4 \times 10^{13}$  Hz (dashed line). The parameters of the split cylinders are those in Fig. 2.

enhanced transmission. This behavior is expected since, as the transmission through the slab increases, the incident waves can penetrate deeper into the slab and interact with the metallic structure.

The transmission and reflection coefficients can be used to determine the effective permittivity and permeability. From these quantities we can then obtain the phase refractive index of the LHM, that is, we can determine the degree to which dispersion affects the negative-index property. To do this, we invert the relations between the transmission and reflection coefficients, and the phase refractive index  $n$  and the impedance  $Z$  of the material [33]

$$T^{-1} = \left[ \cos(nkd) - \frac{i}{2} \left( Z + \frac{1}{Z} \right) \sin(nkd) \right] e^{ikd}, \quad (12)$$

$$\frac{R}{T} = -\frac{i}{2} \left( Z - \frac{1}{Z} \right) \sin(nkd) e^{ikd}, \quad (13)$$

where  $k = \omega/c$  and  $d$  is the thickness of the slab. We point out that the quantities  $T$ ,  $R$ ,  $n$ , and  $Z$  are, in principle, complex, so that  $n$  and  $Z$ , viewed as functions of  $T$  and  $R$ , are multi-valued complex functions (for details, see Ref. [33]). Once  $n$  and  $Z$  are known,  $\epsilon_{\text{eff}}$  and  $\mu_{\text{eff}}$  are given by the relations  $\epsilon_{\text{eff}} = n/Z$  and  $\mu_{\text{eff}} = nZ$ . The results obtained by this procedure are illustrated in Fig. 4. For frequencies within the first band gap,  $\mu_{\text{eff}}$  of the SRR lattice exhibits the necessary resonant behavior to obtain a LHM. Moreover, there is a good agreement between the numerical data and the analytical expression given by Eq. (1). Thus, by using this expression to fit the data, we obtained the following values:  $F = 0.2$  (the analytical value is  $F = 0.24$ ),  $\omega_0 = 1.489 \times 10^{14}$  Hz, and  $\Gamma = 2.4 \times 10^{12}$  Hz.

Although not shown here, we have calculated similar transmission and reflection curves for the thin wire network used in LHM. Again in this case, metallic dielectric constant  $\epsilon_m$  for the wires was assumed to be that given by Eq. (11),

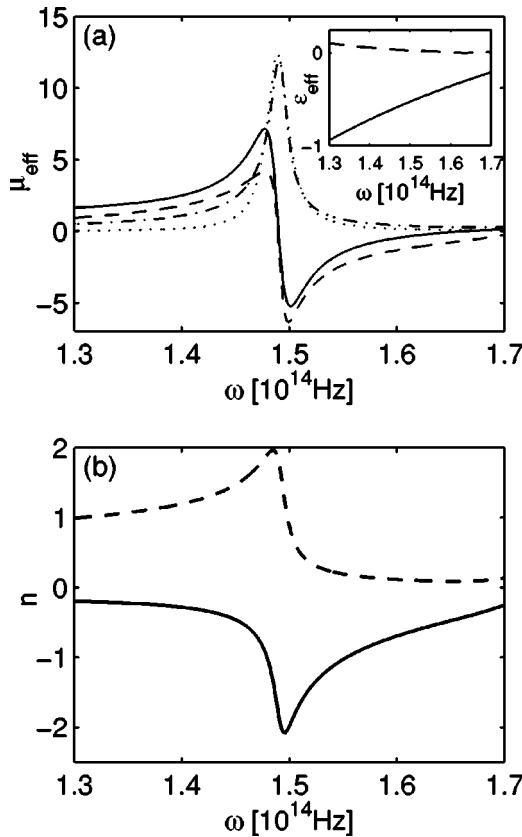


FIG. 4. Dependence  $\mu_{\text{eff}}(\omega)$  of a lattice of SRRs (a) and the real (—) and imaginary (- - -) parts of the refractive index  $n(\omega)$  (b) of the combined structure made of SRRs and wires. The curves in (a) correspond to the real (—) and imaginary ( $\cdots$ ) parts of  $\mu_{\text{eff}}$ , obtained by using TMM, and the real (- - -) and imaginary (- - -) parts of  $\mu_{\text{eff}}$ , obtained by fitting the data to Eq. (1). In the inset, the real (—) and imaginary (- - -) parts of  $\epsilon_{\text{eff}}(\omega)$  for a distribution of parallel wires. The radius of the wires is  $r_w=0.5 \mu\text{m}$  and the parameters of the SRR lattice are the same as those in Fig. 2.

i.e., the Drude expression. Then, through the same procedure we calculated  $\epsilon_{\text{eff}}$  for this structure, and the real part of  $\epsilon_{\text{eff}}$  (as a function of frequency) is presented in the inset in Fig. 4(a). It illustrates that, over this frequency range, the permittivity is negative. We mention that, over the same frequency range, the imaginary part of the permittivity  $\epsilon_{\text{eff}}$  is almost zero. Note that this permittivity  $\epsilon_{\text{eff}}$  can also be fit to a Drude-like expression. Furthermore, it has been demonstrated [33] that the addition of the wires does not change the effective permeability of the resulting LHM, whereas the lattice of SRRs changes only slightly the effective permittivity of the wire mesh. Therefore, with a very good approximation, the effective permittivity and the effective permeability of the LHM will be those shown in Fig. 4(a), that is,  $\epsilon_{\text{eff}}$  and  $\mu_{\text{eff}}$ , respectively. Now having computed both  $\epsilon_{\text{eff}}$  and  $\mu_{\text{eff}}$  for the LHM, we can obtain a plot of  $n$  vs  $\omega$ . Thus, the real and imaginary parts of the refractive index of the combined structure, SRRs and wires, is shown in Fig. 4(b). As indicated, for frequencies near the resonant frequency, the real part of the refractive index is negative. Moreover, Fig. 4(b) illustrates that for frequencies smaller than the resonant frequency  $\omega_0$  the imaginary part of the refractive index can

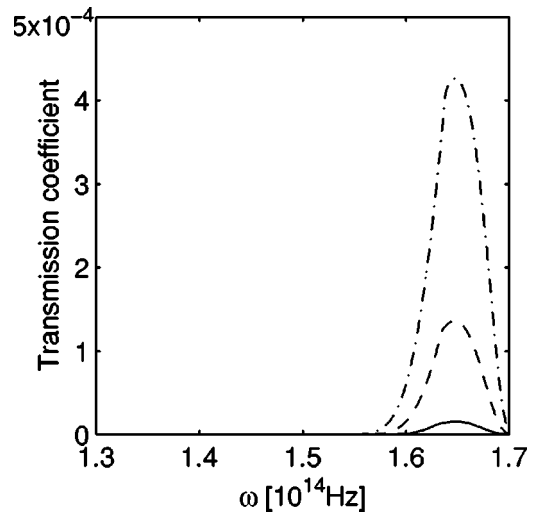


FIG. 5. The transmission coefficient for a homogeneous slab of LHM with thickness  $d=16a$  (16 layers) and effective parameters  $\epsilon_{\text{eff}}(\omega)$  and  $\mu_{\text{eff}}(\omega)$  calculated numerically by TMM. The plasma frequency is  $\omega_p=7.5 \times 10^{15}$  Hz and damping frequency  $\gamma=10^{13}$  Hz (dash-dotted line),  $\gamma=2 \times 10^{13}$  Hz (dashed line), and  $\gamma=4 \times 10^{13}$  Hz (continuous line). The parameters of the split cylinders are the same as those in Fig. 1, the radius of the wires is  $r_w=0.5 \mu\text{m}$ , and the lattice constant is  $a=5 \mu\text{m}$ .

have large values, a characteristic that can have deleterious effects on the properties of the LHM [40]. However, for frequencies larger than the resonant frequency  $\omega_0$ , the imaginary part of the refractive index almost vanishes.

Having the effective values of the electric permittivity and magnetic permeability, we can investigate an important characteristic of the LHM, namely, its transmission property. To do this, we considered a slab with  $M=16$  layers and a width  $d=Ma$ . Then, by using the values of the effective electric permittivity and magnetic permeability determined with TMM, for several different values of the damping plasma frequency, we calculated the transmission coefficient through the slab [41]. The results are presented in Fig. 5. This figure illustrates that, for these parameters, the transmission coefficient through the slab is small and, thus, the absorption in the LHM is strong. Note, however, that the transmission in the LHM is improved sharply over the case in which only rings are considered (see Fig. 2). Figure 5 also shows that the transmission coefficient through the slab is strongly dependent on losses  $\gamma$  in the metal. Thus, it is possible to considerably reduce the losses in the LHM slab by using a lower loss metal in the LHM; for instance, if silver is used,  $\gamma_{\text{Ag}}=4.35 \times 10^{12}$  Hz, the transmission coefficient will be improved by more than an order of magnitude. Moreover, although not examined here in detail, it is clear that a careful optimization of the parameters in the geometry of the LHM can also sharply improve the transmission of the LHM. For example, as will be shown in the following section, changing the radius of the wires improves considerably the transmission properties of the metamaterial.

Our results in Fig. 4(a) show that, surprisingly, the LHM is magnetically active, that is,  $\mu_{\text{eff}} \neq 1$ , at frequencies  $\omega \sim 10^{14}$  Hz. In the case of the metamaterial discussed here,

the magnetic activity is the result of the onset of resonant currents in the split rings induced by the magnetic field of the incoming wave. Thus, the time varying external magnetic field induces electrical currents that flow around the metallic rings and, as a result, a magnetic moment is created. In addition, the capacitance associated with the narrow gap between the rings, combined with the inductance of the rings, determines a resonant response of the structure. When the dimensions of the split rings are scaled down, the resonant frequency determined by the inductance of the rings and their capacitance can reach the frequency range shown here. As it is shown below, we verify this fact by estimating the resonant frequency of the rings, based on the values of their geometrical parameters. Furthermore, it has been demonstrated that if the characteristic dimensions of rings, arranged in a slightly different pattern from the one discussed here, are of the order of tens of nanometers, the characteristic resonant frequency and, consequently, the frequency at which the metamaterial becomes magnetically active can reach optical frequencies [42]. Note that this approach, which uses an artificial or metamaterial, is different from well known examples, even at optical frequencies, of magnetically active materials. For instance, in the case of ferromagnetic garnets, the off-diagonal tensor components of the permittivity and permeability are comparable at visible wavelengths [43]. In addition, recently, it has been demonstrated that other types of metallodielectric composites, made of metallic nanowires embedded in a dielectric matrix, can have magnetic properties at optical frequencies [21,44]. In such a case, the magnetic moments of the currents induced in the nanowires as well as the displacement currents between the nanowires are responsible for the magnetic response of the composite. In a different scheme, by inserting nanoscale particles of ferromagnetic metals in an insulating matrix, the so called cermets, one obtains a composite material that is magnetically active up to infrared frequencies [45]. In the rest of this section, we will discuss in more detail the dependence of the resonant frequency of the rings on the material parameters of the metal.

Furthermore, we analyzed in more detail the influence of the parameters describing the dielectric function of the metal (plasma frequency and the damping frequency) on the position and size of the first band gap in the transmission coefficient. The results are presented in Fig. 6. As seen in Fig. 6(a), as the plasma frequency  $\omega_p$  increases, the midgap frequency increases asymptotically to a constant limit. Also, notice that as the plasma frequency increases the absolute value of the dielectric function  $\epsilon_m$  increases, too. A similar behavior has been observed in Ref. [32], that is, for large absolute values of the dielectric function the resonant frequency of the SRR reaches an asymptotic limit. However, in the case studied in Ref. [32], the dielectric function did not depend on the frequency.

An explanation for this phenomenon is as follows. Equation (11) can be recast in the form

$$\epsilon_m = 1 + i \frac{\sigma}{\omega \epsilon_0}, \quad (14)$$

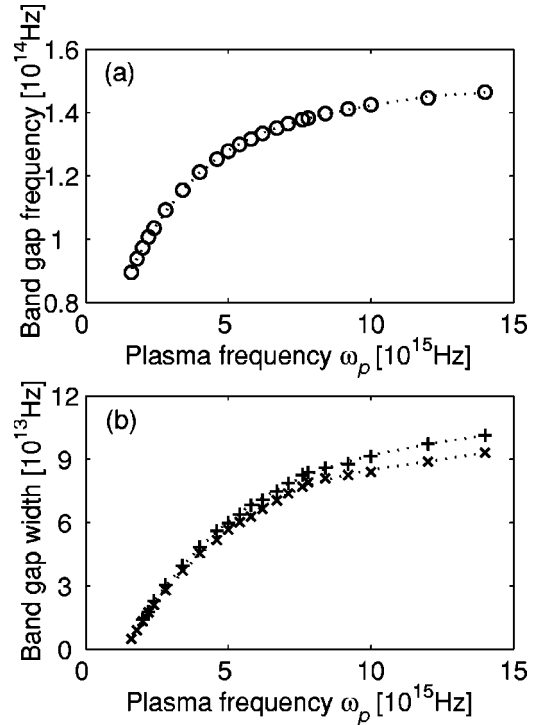


FIG. 6. The dependence of the position and width of the first band gap on the metal parameters: (a) the band gap frequency vs the plasma frequency  $\omega_p$ ; (b) the band gap width vs the plasma frequency  $\omega_p$  in the lossless case  $\gamma=0$  (crosses) and with losses  $\gamma = 10^{13}$  Hz (pluses). The parameters of the SRR are the same as those in Fig. 1 and the lattice constant is  $a=5 \mu\text{m}$ . In both figures, the dotted lines are only a guide to the eye.

where

$$\sigma = \frac{i \epsilon_0 \omega_p^2}{\omega + i \gamma} \quad (15)$$

is the frequency-dependent conductivity and  $\epsilon_0$  is the vacuum permittivity. Combining Eqs. (15) and (1), one obtains an expression for the resonant frequency of the rings in terms of the metallic plasma frequency and SRR's dimensions:

$$\tilde{\omega}_0 = \frac{\omega_0}{\sqrt{1 + \frac{2c^2}{wr\omega_p^2}}}. \quad (16)$$

Thus, the resonant frequency  $\tilde{\omega}_0$  is an increasing function of the plasma frequency  $\omega_p$  and reaches the asymptotic value  $\omega_0$  as the plasma frequency goes to infinity. Moreover, we observed that the midgap frequency does not depend on the damping frequency  $\gamma$ , a result that is also in agreement with Eq. (16). Finally, Eq. (16) shows that the plasma frequency  $\tilde{\omega}_p$ , above which the resonant frequency  $\tilde{\omega}_0$  reaches  $1/\sqrt{2}$  of the asymptotic value  $\omega_0$  is given by

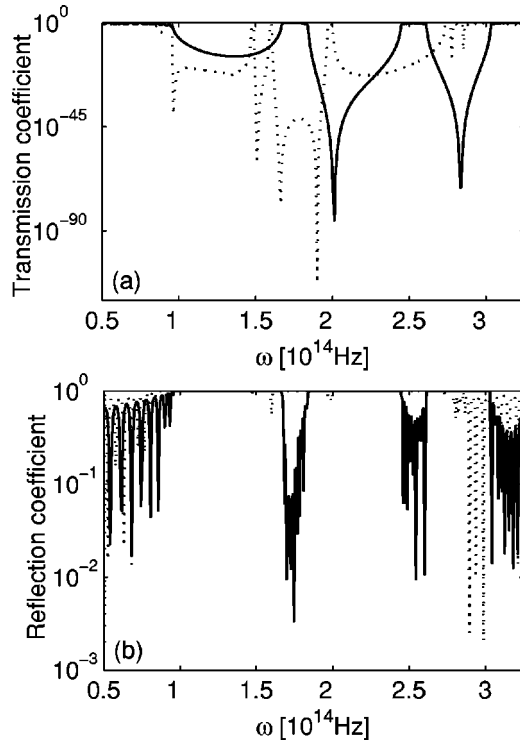


FIG. 7. The transmission coefficient (a) and reflection coefficient (b) for a slab of  $M=16$  layers of split-ring resonators (continuous line) and split-square resonators (dotted line). The plasma frequency is  $\omega_p=7.5 \times 10^{15}$  Hz and the damping frequency  $\gamma=0$ . The parameters of the resonant structures are the same as those in Fig. 1 and the lattice constant is  $a=5 \mu\text{m}$ .

$$\bar{\omega}_p = \sqrt{\frac{2c^2}{w_r}} \approx 7.35 \times 10^{14} \text{ Hz}, \quad (17)$$

a value that is in close agreement with the data in Fig. 6(a).

In Fig. 6(b) we present the width of the first band gap as a function of plasma frequency, calculated for two cases: for a lossless metal and for a metal characterized by the damping frequency  $\gamma=10^{13}$  Hz. As expected, the band gap width changes with the damping frequency. More exactly, our calculations show that it increases weakly with  $\gamma$ . Moreover, this figure shows that the band gap frequency width increases with the plasma frequency  $\omega_p$ .

We have also investigated the dependence of the transmission properties of the material slab on the geometry of its building blocks. Thus, two cases were taken into account: the slab consists of a lattice of split rings (as in the previous discussion) or split squares. In order to be able to compare the results, the two resonant structures were chosen to have similar dimensions. The results are shown in Fig. 7.

Several conclusions can be drawn from the results presented in this figure. First, one can observe that the structure of the band gaps in the transmission coefficient is strongly dependent on the geometry of the resonant building blocks. Thus, when the unit cell contains split-square resonators, the transmission coefficient contains more gaps and these gaps have a larger depth. Furthermore, in the case of split-square resonators, one can observe at the edges of some of the gaps

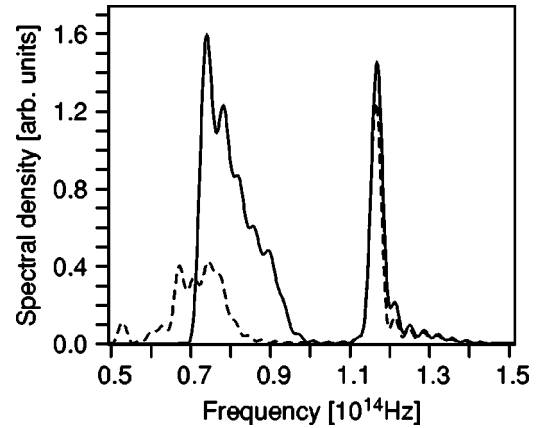


FIG. 8. Transmission through  $M=4$  layers of split squares (dashed line), and split squares and wires (continuous line). The real part of the refractive index of the metal at the reference frequency  $\omega_{\text{ref}}=1.26 \times 10^{14}$  Hz is  $n_r=1.5$  and the absorption  $\alpha=15$ . The parameters of the structures are  $r=1.5 \mu\text{m}$ ,  $g=0.4 \mu\text{m}$ ,  $s=0.4 \mu\text{m}$ ,  $w=0.8 \mu\text{m}$ , the thickness of the squares  $t=0.8 \mu\text{m}$ , the transverse width of the wires  $d=0.8 \mu\text{m}$ , and the lattice constant is  $a=8 \mu\text{m}$ .

very sharp dips, an indication of large densities of states at these edge frequencies. A similar phenomenon has been recently observed experimentally when the transmission at near-infrared frequencies through a 3D metallic photonic crystal has been measured [46].

### B. FDTD based computations

Although TMM method is a very powerful tool in characterizing the band structure of periodic structures, due to the fact that it operates in the wave vector space, it cannot provide information on the temporal dynamics of the interaction between electromagnetic waves and periodic structures. In contrast, the FDTD method is a time-domain method, so that it is very powerful in describing the time evolution of the electromagnetic field interacting with periodic structures. In particular, it can provide a detailed and accurate description of the electromagnetic fields in the presence of metallic structures. Because of this capability, we also used the FDTD method to investigate the response of a slab of LHM to a pulse of electromagnetic waves that propagates perpendicularly to the slab. The fact that we were able to implement 3D calculations with the FDTD code also made using it desirable.

Using FDTD, we were able to start directly with the transmission properties of a *combined* 3D periodic structure of split squares and wires. The wires were along the  $x$  axis and the split squares were arranged in the  $x$ - $z$  plane. The dimensions of the structures were generally comparable to those used in the preceding section. However, the split squares were now  $t=0.8 \mu\text{m}$  in thickness. Further details on the exact dimensions are given in the caption of Fig. 8. We chose 3D split squares and wires with a rectangular transverse section because such shapes are better approximated by a rectangular spatial grid, allowing us to use a relatively small number of grid points. The slab contained  $M=4$  layers.

In order to find the transmission through such a structure, we launched a Gaussian pulse which propagates along the  $z$

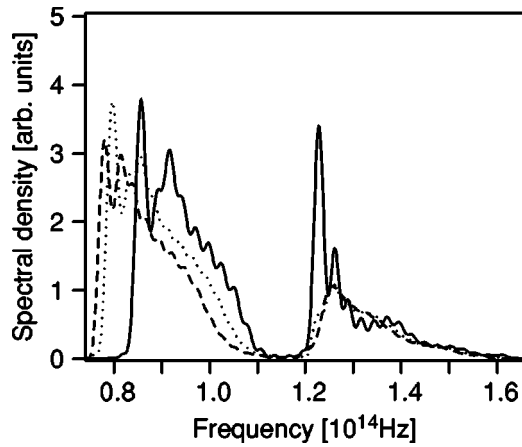


FIG. 9. Transmission through  $M=4$  layers of split squares and wires. The parameters of the split squares were chosen as in Fig. 8, whereas the transverse width of the wires is  $d=1.75 \mu\text{m}$  (continuous line),  $d=1 \mu\text{m}$  (dotted line), and  $d=0.5 \mu\text{m}$  (dashed line).

axis and with spectral width equal to half of its central frequency. The pulse was centered at a wavelength  $\lambda = 25 \mu\text{m}$ . The incident wave was  $s$  polarized, with the magnetic field along the axis of the split squares. To model the frequency dispersion of the metal we used Eqs. (9) and (10), with reference frequency  $\omega_{\text{ref}}=1.26 \times 10^{14}$  Hz. The real part of the refractive index was  $n_r=1.5$  and the absorption  $\alpha = 15$ . At the other side of the slab we recorded the values of the electric and magnetic fields. The simulation was run until the response of the structure became negligibly small and the recorded data was then Fourier transformed. We performed these numerical calculations in two cases, that is, first when only the split squares were included and second with both the split squares and the wires. The results are presented in Fig. 8. As seen in this figure, there is a band gap in the transmission through the slab at a frequency that corresponds to  $\lambda \approx 20 \mu\text{m}$ . The larger value for the band gap wavelength, as compared to the one obtained by the TMM, is due to the fact that in the case analyzed by TMM the lattice constant was smaller. Furthermore, Fig. 8 shows that, when the network of wires is added, the transmission through the slab is significantly enhanced, and the band gap is almost halved, with an increased transmission at frequencies closer to the lower band edge. A similar behavior has been observed both in experiments performed at microwave frequencies and in numerical simulations.

In order to study in more detail the effects of the wire mesh on the transmission properties of the LHM, we repeated the numerical simulations on the full structure, but for different values of the radius of the wires; all other parameters were kept constant. Figure 9 shows the transmission spectra through  $M=4$  layers of split squares and wires, for three different values of the radius of the wires. This figure illustrates that as the radius of the wires decreases, the transmission through the LHM slab decreases and the slab becomes more absorbing. This effect is consistent with a similar behavior for losses of wire meshes in the microwave region, which has been recently reported in Ref. [47], and is explained by the fact that the imaginary part of the effective

permittivity of a mesh of metallic wires increases considerably when the radius of the wires is decreased. Consequently, for thinner wires, the imaginary part of the refractive index of the LHM obtained by adding the split rings is larger, so that the absorption losses of the metamaterial are larger. This fact shows that the geometrical characteristics of the building blocks of the LHM play an important role in defining its optical properties.

The FDTD method allowed us to calculate directly the electromagnetic field created by a monochromatic wave that propagates perpendicularly onto a slab of LHM. Both 2D and 3D geometries were considered, and in both cases periodic boundary conditions in the transverse directions were imposed. In Fig. 10 we present the field components that correspond to the 2D geometry. The bright (dark) gray regions correspond to low (high) field intensities. As before, the incident plane wave was  $s$  polarized, so that the only nonzero field components were  $H_y$ ,  $E_x$ , and  $E_z$ . As this figure illustrates, there is an intense induced magnetic field along the ring's axis, field which induces surface currents in both rings, which flow in the opposite directions. This fact is best illustrated by the distribution of the electric fields  $E_x$  and  $E_z$ . Also, notice that due to the fact that we deal with metals, the fields do not penetrate into the rings. This fact shows that, at infrared or optical frequencies, skin effects play an important role. Furthermore, since the electromagnetic field does not penetrate into the metal, there is a significant enhancement of the field in the narrow regions between metallic domains, e.g., between the two rings or in the slit regions. This effect can lead to a strong enhancement of the nonlinear response of the metamaterial.

We extended this analysis to a full 3D structure and the results are shown in Fig. 11. In this case, a network of wires was added to the periodic structure of metallic split squares. As in the previous case, we determined the electromagnetic field induced by a plane wave, which propagates perpendicularly on a slab of three layers of split squares. Since in this case the lattice constant is larger than that in the case of SRRs, the wavelength of the incident wave was  $\lambda = 20 \mu\text{m}$ . The plane wave was again  $s$  polarized, with the electric field oriented along the wires. As in the 2D case, the field distributions in Fig. 11 illustrate the resonant behavior of the split-square structure. The results also show a strong magnetic field around the wires, field created by the inductive currents flowing along the wires. Moreover, in this case, too, one can observe high intensities of the electromagnetic fields in the narrow regions between metallic domains, an effect that can lead to enhanced nonlinear response of the LHM.

## V. CONCLUSIONS

We have investigated the properties of recently introduced metallic LHM at infrared and optical frequencies. Both the TMM and the FDTD method have been employed and the results obtained by using the two methods have been compared. The transmission, reflection, and absorption of a slab of metamaterial was calculated numerically and the relationship between the properties of the photonic gaps displayed

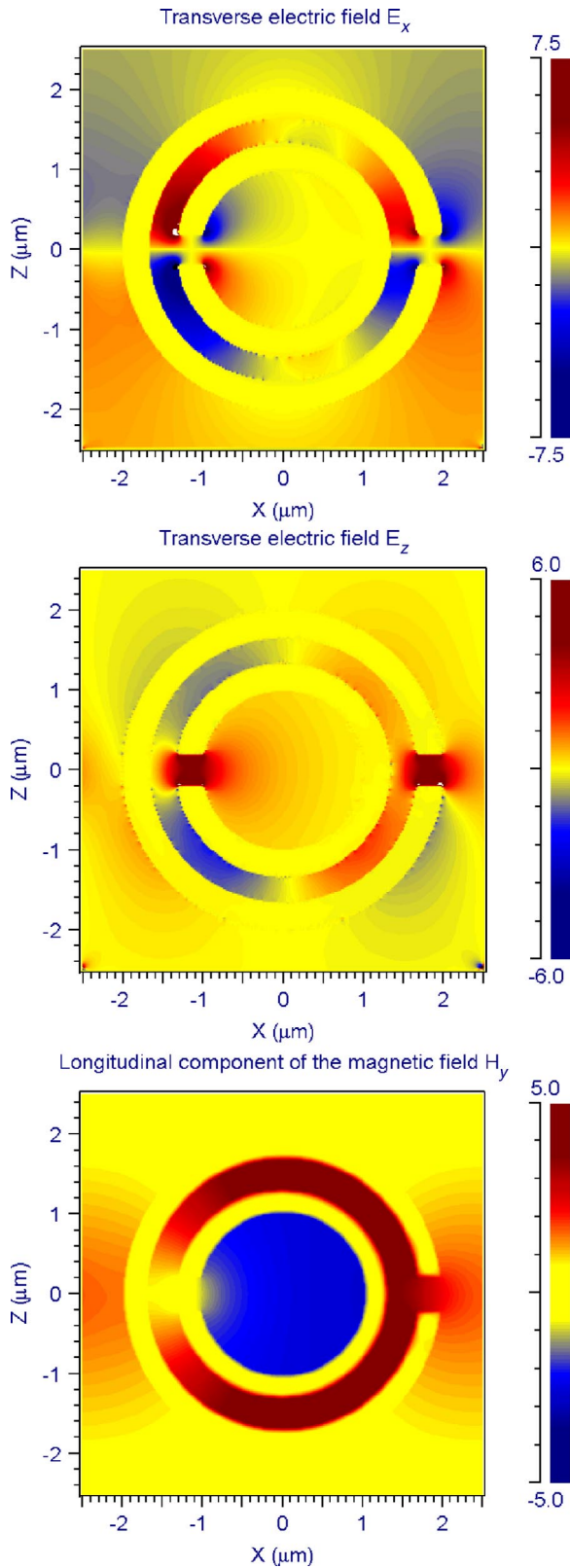


FIG. 10. (Color online) The field components created by a plane wave at normal incidence on a layer of split cylinders. The real part of the refractive index of the metal is  $n_r=1.5$ , the absorption  $\alpha =15$ , and the wavelength of the incident wave  $\lambda=15 \mu\text{m}$ . The parameters of the resonant structures are the same as those in Fig. 1 and the lattice constant is  $a=5 \mu\text{m}$ .

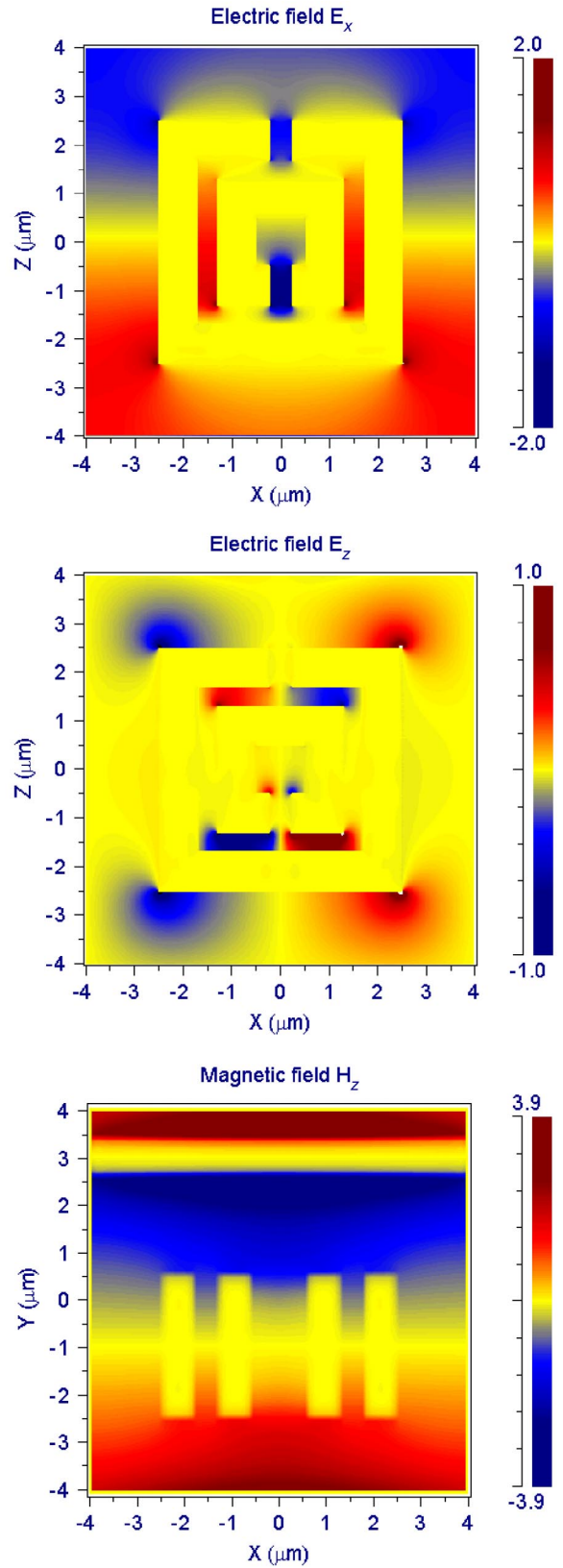


FIG. 11. (Color online) The field components created by a plane wave at normal incidence on a layer of split squares and metallic wires. The wavelength of the incident wave  $\lambda=20 \mu\text{m}$  and the parameters of the structures are the same as those in Fig. 8.

by these coefficients and the dispersive properties of the metal was established. Thus, we showed that as the plasma frequency increases, the frequency at which it is expected that such a material exhibits a negative refraction index increases asymptotically to a frequency limit determined entirely by the geometry of the resonant structure. A theoretical explanation of this effect has been proposed. On the other hand, it has been shown that the position of the band gap responsible for the negative-refractive-index behavior is independent of the damping frequency of the metal.

The calculated transmission and reflection coefficients also allowed us to calculate the effective permittivity, the effective permeability, and the refractive index. The calculations showed that the refractive index is negative near the resonant frequency of the metallic rings, frequency that corresponds to a band gap in the transmission spectrum.

Also, numerical investigations based on the FDTD method of 2D and 3D periodic distributions of SRR and metallic wires have been performed and the results obtained by this method agreed with those obtained by the TMM. A field distribution consistent with previously proposed theoretical models has been obtained, confirming thus the magnetically induced resonant behavior of such LHM. Moreover,

it has been demonstrated that, as at the microwave frequencies, adding a mesh of wires to a 3D periodic distribution of split rings determines the transmission coefficient near the resonant frequency to increase, while the width of the band gap is reduced to about a half of its previous value. This suggests that metamaterials with negative refractive index can exist at infrared or even optical frequencies.

While the dimensions required for producing this effect can be challenging for most nanofabrication tools, they are still within the capability of state-of-the-art technology. Thus, the thin metallic structures that are discussed in this paper, with characteristic dimensions of a few hundred nanometers, can be patterned by using deep UV or electron-beam lithography.

#### ACKNOWLEDGMENTS

The authors want to thank Dr. Hongling Rao and Dr. R. Scarmozzino for many useful discussions on the FDTD method. We also thank RSoft, Inc., for making available to us the software package FULLWAVE. This work has been supported by the NIST Advanced Technology Program Cooperative Agreement under Grant No. 70NANB8H4018.

- 
- [1] V.G. Veselago, *Usp. Fiz. Nauk* **92**, 517 (1964) [*Sov. Phys. Usp.* **10**, 509 (1968)].
  - [2] D.R. Smith, W.J. Padilla, D.C. Vier, S.C. Nemat-Nasser, and S. Schultz, *Phys. Rev. Lett.* **84**, 4184 (2000).
  - [3] R.A. Shelby, D.R. Smith, S.C. Nemat-Nasser, and S. Schultz, *Appl. Phys. Lett.* **78**, 489 (2001).
  - [4] R.A. Shelby, D.R. Smith, and S. Schultz, *Science* **292**, 489 (2001).
  - [5] D.R. Smith and N. Kroll, *Phys. Rev. Lett.* **85**, 2933 (2000).
  - [6] J.B. Pendry, A.J. Holden, D.J. Robbins, and W.J. Stewart, *IEEE Trans. Microwave Theory Tech.* **47**, 2075 (1999).
  - [7] J.B. Pendry, A.J. Holden, W.J. Stewart, and I. Youngs, *Phys. Rev. Lett.* **76**, 4773 (1996).
  - [8] J.B. Pendry, A.J. Holden, D.J. Robbins, and W.J. Stewart, *J. Phys.: Condens. Matter* **10**, 4785 (1998).
  - [9] R.M. Walser, A.P. Valanju, and P.M. Valanju, *Phys. Rev. Lett.* **87**, 119701 (2001).
  - [10] J.B. Pendry, *Phys. Rev. Lett.* **85**, 3966 (2000).
  - [11] D.R. Smith, D. Schurig, and J.B. Pendry, *Appl. Phys. Lett.* **81**, 2713 (2002).
  - [12] J. Pacheco, T.M. Grzegorzczuk, B.I. Wu, Y. Zhang, and J.A. Kong, *Phys. Rev. Lett.* **89**, 257401 (2002).
  - [13] N. Garcia and M. Nieto-Vesperinas, *Phys. Rev. Lett.* **88**, 207403 (2002).
  - [14] P.M. Valanju, R.M. Walser, and A.P. Valanju, *Phys. Rev. Lett.* **88**, 187401 (2002).
  - [15] S. Rupin, *Phys. Lett. A* **277**, 61 (2000); *J. Phys.: Condens. Matter* **13**, 1811 (2001).
  - [16] S. Rupin, *Solid State Commun.* **116**, 411 (2000).
  - [17] V. Kuzmiak and A.A. Maradudin, *Phys. Rev. B* **66**, 045116 (2002).
  - [18] R.W. Ziolkowski and E. Heyman, *Phys. Rev. E* **64**, 056625 (2001).
  - [19] F.J. Rachford, D.L. Smith, P.F. Loschialpo, and D.W. Forester, *Phys. Rev. E* **66**, 036613 (2002).
  - [20] G. Dewar, *Int. J. Mod. Phys. B* **15**, 3258 (2001).
  - [21] V.A. Podolskiy, A.K. Sarychev, and V.M. Shalaev, *J. Nonlinear Opt. Phys. Mater.* **11**, 65 (2002).
  - [22] C. Luo, S.G. Johnson, and J.D. Joannopoulos, *Appl. Phys. Lett.* **81**, 2352 (2002).
  - [23] C.J. Chen and R.M. Osgood, *Phys. Rev. Lett.* **50**, 1705 (1983).
  - [24] T.W. Ebbesen, H.J. Lezec, H.F. Ghaemi, T. Thio, and P.A. Wolff, *Nature (London)* **391**, 667 (1998); H.J. Lezec, A. Degiron, E. Devaux, R.A. Linke, L. Martin-Moreno, F.J. Garcia-Vidal, and T.W. Ebbesen, *Science* **297**, 820 (2002).
  - [25] A. Moroz, *Phys. Rev. Lett.* **83**, 5274 (1999).
  - [26] D.F. Sievenpiper, M.E. Sickmiller, and E. Yablonovitch, *Phys. Rev. Lett.* **76**, 2480 (1996).
  - [27] J.A. Porto, F.J. Garcia-Vidal, and J.B. Pendry, *Phys. Rev. Lett.* **83**, 2845 (1999); F.J. Garcia-Vidal and L. Martin-Moreno, *Phys. Rev. B* **66**, 155412 (2002).
  - [28] L. Martin-Moreno, F.J. Garcia-Vidal, H.J. Lezec, K.M. Pellerin, T. Thio, J.B. Pendry, and T.W. Ebbesen, *Phys. Rev. Lett.* **86**, 1114 (2001).
  - [29] D.F. Sievenpiper, L. Zhang, R.F.J. Broas, N.G. Alexopolous, and E. Yablonovitch, *IEEE Trans. Microwave Theory Tech.* **47**, 2059 (1999).
  - [30] J.B. Pendry and A. MacKinnon, *Phys. Rev. Lett.* **69**, 2772 (1992).
  - [31] J.B. Pendry, *J. Mod. Opt.* **41**, 209 (1994); P.M. Bell, J.B. Pendry, L.M. Moreno, and A.J. Ward, *Comput. Phys. Commun.* **85**, 306 (1995).
  - [32] P. Markos and C.M. Soukoulis, *Phys. Rev. B* **65**, 033401 (2001); *Phys. Rev. E* **65**, 036622 (2002).
  - [33] D.R. Smith, S. Schultz, P. Markos, and C.M. Soukoulis, *Phys. Rev. B* **65**, 195104 (2002).

- [34] I. El-Kady, M.M. Sigalas, R. Biswas, K.M. Ho, and C.M. Soukoulis, *Phys. Rev. B* **62**, 15 299 (2000).
- [35] K.S. Yee, *IEEE Trans. Antennas Propag.* **14**, 302 (1966).
- [36] A. Taflove and S.C. Hagness, *Computational Electrodynamics: The Finite-Difference Time-Domain Method* (Artech House, Boston, 2000).
- [37] J.B. Judkins and R.W. Ziolkowski, *J. Opt. Soc. Am. A* **12**, 1974 (1995).
- [38] See <http://www.rsoftdesign.com>
- [39] M.A. Ordal, L.L. Long, R.J. Bell, S.E. Bell, R.R. Bell, R.W. Alexander, Jr., and C.A. Ward, *Appl. Opt.* **22**, 1099 (1983); M.A. Ordal, R.J. Bell, R.W. Alexander, Jr., L.L. Long, and M.R. Querry, *ibid.* **24**, 4493 (1983).
- [40] N. Garcia and M. Nieto-Vesperinas, *Opt. Lett.* **27**, 885 (2002).
- [41] M. Born and E. Wolf, *Principles of Optics* (Cambridge University Press, Cambridge, 1997).
- [42] S. O'Brien and J.B. Pendry, *J. Phys.: Condens. Matter* **14**, 6383 (2002).
- [43] S. Wittekoek and D.E. Lacklison, *Phys. Rev. Lett.* **28**, 740 (1972); G.S. Krinchik, V.A. Krylova, E.V. Beredennikova, and R.A. Petrov, *Zh. Eksp. Teor. Fiz.* **65**, 715 (1973) [*JETP* **38**, 354 (1974)].
- [44] A.N. Lagarkov and A.K. Sarychev, *Phys. Rev. B* **53**, 6318 (1996).
- [45] M. Gadenne, in *Optical Properties of Nanostructured Random Media, Topics in Applied Physics Series*, edited by V. M. Shalaev (Springer-Verlag, Berlin, 2002).
- [46] J.G. Fleming, S.Y. Lin, I. El-Kady, R. Biswas, and K.M. Ho, *Nature (London)* **417**, 52 (2002).
- [47] E.V. Ponizovskaya, M. Nieto-Vesperinas, and N. Garcia, *Appl. Phys. Lett.* **81**, 4470 (2002); N. Garcia, E.V. Ponizovskaya, and J.Q. Xiao, *ibid.* **80**, 1120 (2002).